ELSEVIER

Journal of Magnetism and Magnetic Materials 191 (1999) 301–312

Journal of magnetism and magnetic materials

Exchange coupling in Co/Cu/Co sandwiches studied by spin-polarized low energy electron microscopy

T. Duden, E. Bauer*

Department of Physics and Astronomy, Arizona State University, Tempe, AZ 85287-1504, USA

Received 24 June 1998; received in revised form 4 September 1998

Abstract

The evolution of the magnetic domain structure of Co/Cu/Co sandwiches epitaxially grown on a W(1 1 0) surface under UHV conditions is studied in situ by spin-polarized low energy electron microscopy as a function of the Cu spacer and Co top layer thickness in the thickness range from 2 to 9 monolayers Cu and 1 to 7 monolayers Co. The various coupling modes are correlated with the microstructure of the layers as observed by low energy electron microscopy.

PACS: 75.70.Cn; 75.70.Kw; 75.30.Et

Keywords: Exchange coupling; Sandwiches; Microstructure; SPLEEM; Mean free path

1. Introduction

The exchange interaction between ferromagnetic layers separated by a nonmagnetic spacer layer has been the subject of intensive study for nearly a decade, driven in part by its fundamental interest but mainly by its importance for the understanding of the giant magnetoresistance (GMR) which has important applications in magnetic storage and sensing devices. In layered systems GMR can occur when the magnetization in alternating layers is antiparallel, that is when the exchange coupling is antiferromagnetic (AF). For a given ferromagnetic layer thickness this occurs at certain spacer thicknesses which are determined by the Fermi surface of the spacer material. Many theoretical treatments of this problem have been published (for references see Refs. [1,2]), the most flexible being the quantum well or quantum interference model [1].

A large GMR is to be expected when the band structure of the majority electrons near the Fermi surface is similar to the band structure of the spacer material and the band structure of the minority electrons is quite different and vica versa. The system Co/Cu is particularly favorable from this point of view. Some of the highest GMR effects have indeed been observed in sputtered Co/Cu multilayers. In Co/Cu multilayers grown by molecular beam epitaxy (MBE) AF coupling and GMR have

* Corresponding author. Tel.: + 1-602-965-2993; fax: + 1-602-965-7954; e-mail: bauer@asu.edu.

0304-8853/99/$ – see front matter
PII: S0304-8853(98)00363-1

been more elusive, in particular in layer systems with (1 1 1) orientation. This has led to numerous studies of these systems (for references see Refs. [3–5]) with the result that AF coupling and GMR are extremely sensitive to the microstructure of the layers. No significantly reduced or incomplete AF coupling have been reported for MBE grown films and only recently completely AF coupled sandwiches could be grown [6,7] using a surfactant which improved layer-by-layer growth and suppressed stacking fault formation [8].

The strong interrelation between exchange coupling and microstructure which is evident from numerous laterally averaging ex situ studies makes it desirable to correlate on one and the same layer system in situ the magnetic domain structure – which reflects the coupling – and the microstructure. This can be done best by spin-polarized low energy electron microscopy (SPLEEM) [9]. This method combines the diffraction and interference contrast mechanism of low energy electron microscopy (LEEM) [10,34] with the magnetization ($\boldsymbol{M}$) sensitivity provided by the exchange interaction between the target electrons and the beam electrons with spin polarization $\boldsymbol{P}$. The most important LEEM contrast mechanism in the present context are the quantum size contrast, which allows to determine local thickness variations in the growing layers with atomic depth sensitivity, and the step contrast which allows to image substrate steps down to atomic height. The magnetic contrast – which is usually weak – is proportional to $\boldsymbol{P}\cdot\boldsymbol{M}$ and superimposed on the structural contrast but can be obtained in pure form by producing the difference image between images taken with opposite $\boldsymbol{P}$. The intimate relation between microstructure and magnetic domain structure has been demonstrated in this manner for example for epitaxial Co layers on a W(1 1 0) surface [11]. An important aspect is that these studies can be made in situ while the film system is growing.

Preliminary SPLEEM studies of the exchange coupling in Co/Cu/Co sandwiches [12] have already shown that at the Cu thickness for which AF coupling has been reported in the past the domain pattern of the overlayer was much more complicated than expected in the case of AF coupling. At the time when these studies were made only the in-plane components of the magnetization could be imaged. The addition of a spin manipulator [13] allows now to image all three components so that the direction of $\boldsymbol{M}$ can be completely determined at the present lateral routine resolution of several tens of nanometers. With this addition we have made a systematic study of the dependence of the magnetic domain structure of Co/Cu/Co sandwiches upon the thickness of the spacer layer and the top Co layer in order to obtain a deeper insight in the relationship between exchange coupling and microstructure.

2. Experimental

The experiments were performed in the orginal LEEM instrument described in Ref. [36] in which the original field emission gun was replaced by a spin polarized illumination system with polarization manipulator (see also Fig. 3 in Ref. [9]). The base pressure of the instrument was 2×10^{-10} Torr. During the depositions the pressure stayed in the 10^{-10} Torr range and was typically around 6×10^{-10} Torr. The W(1 1 0) crystal could be heated from the back side by radiation up to 500 K and by electron bombardment up to 2000 K. It was precleaned by heating for several hours in an oxygen atmosphere at a partial pressure of about 2×10^{-6} Torr. Between the experiments it was cleaned regularly by annealing at approximately 1400 K in 5×10^{-7} Torr oxygen for 30 min, followed by flashing to 2000 K in UHV. Criteria for a clean surface were (i) the absence of W carbide segregation at surface imperfections upon annealing at about 1300 K and (ii) step flow growth of the first Co monolayer during the deposition at 750 K. This growth pattern is very sensitive to surface contamination by segregated or adsorbed impurities which cause pinning of the growth fronts and nucleation on the terraces. The first monolayer is filled in two steps: first, a pseudomorphic (ps) monolayer is formed in which close-packed (cp) islands nucleate and grow until the cp monolayer is completed. The completion of the ps and the cp monolayer provides a precise rate calibration before each experiment. After completion of the cp monolayer the temperature was reduced to about

400 K and the deposition continued to the desired thickness (7 ML). At this temperature the mobility is high enough and the two-dimensional nucleation rate low enough so that large terraces form (several 100 nm diameter) which show pronounced thickness dependent quantum size contrast. This contrast allows the observation of the completion of consecutive layers and the characterization of the roughness of the Co film. Once the desired Co film thickness was reached, the heating was turned off. After the temperature had dropped to values slightly above room temperature Cu was deposited as a spacer layer. The Cu rate was calibrated before the Co deposition by the time needed to form 1 ML. While the completion of the first monolayer is well observable the next two layers seem to grow in double layer islands. The top Co layer was deposited in ML doses. Typical deposition rates were 1/8 ML/min both for Co and Cu.

After each monolayer dose, a measurement cycle was performed to monitor the resulting magnetic structure. The images were acquired from the final screen using a CCD camera. For each magnetic image, two images resulting from the average of 64 consecutive video frames were taken. Between each single image the polarization vector of the incident electron beam was inverted. The magnetic signal was then obtained by a normalized subtraction using the formula

$$A = 127 + 100K\,(I_+ - I_-)/(I_+ + I_-),$$

where A is the normalized asymmetry, K a contrast enhancement factor ranging from 7 to 15 and I_+, I_- are the intensities for the images with opposite spin polarization. The direction of $\boldsymbol{M}$ can be determined to better than $\pm 3^\circ$ by maximizing/minimizing the magnetic contrast which is proportional to $\boldsymbol{P}\cdot\boldsymbol{M}$. The direction of $\boldsymbol{P}$ which is needed for this determination is calibrated using films with strong perpendicular $\boldsymbol{M}$ (4 ML Co/Au(1 1 1)) and strong in-plane anisotropy (Co/W(1 1 0)). For arbitrary angles $\boldsymbol{P}$ is obtained from the $\boldsymbol{P}\cdot\boldsymbol{M}$ dependence of the contrast in these layers. Initially the relationship between the direction of $\boldsymbol{P}$ and the settings of the spin manipulator were determined with a Mott detector [13].

3. Results

The experiments were performed for Cu spacer thicknesses ranging from 2 to 9 ML in 1 ML steps with intermediate values of 4.25 and 4.5 ML in the AF coupling region. The kind of SPLEEM images obtained during a typical experiment is illustrated in Fig. 1 for a few selected thicknesses of the top Co layer. In this example the Cu spacer is 8 ML thick. The three columns show the lateral distribution of the three $\boldsymbol{M}$ components obtained with $\boldsymbol{P}$ parallel to W[1 $\bar{1}$ 0], W[0 0 1] and W[1 1 0] from the left to the right. The easy in-plane axis of the bottom Co layer is along the W[1 $\bar{1}$ 0] direction but there is also a weak out-of-plane component ($M_\perp/M_\parallel \approx 1:6$ [11]). The images in row (a) are taken from the bottom Co layer covered with 8 ML Cu. The $\boldsymbol{M}$ distributions are completely identical with those of the bare Co layer, only the signal/noise ratio is reduced by the spin-independent attenuation in the Cu layer. 1 ML Co on top strongly reduces the contrast and at 2 ML Co the magnetic contrast has disappeared nearly completely (not shown). At 3 ML Co strong contrast appears in the [0 0 1] (90°) image with a completely different $\boldsymbol{M}$ distribution while only very weak contrast is seen in the [1 $\bar{1}$ 0] (0°) image (row b). At 4 ML Co (row c) the contrast in the 0° image has increased considerably and continues to do so with increasing Co thickness while the contrast in the 90° image decreases beyond 4 ML as seen in the 7 ML Co images (row d).

This change of the domain structure with top Co layer thickness, in which the 90° component appears first with increasing thickness is characteristic for 3, 4, 8 and 9 ML thick spacer layers but at 6 and 7 ML Cu the 0° component develops faster than the 90° component. At 4.25 and 4.5 ML both appear simultaneously and at 5 ML no clear decision can be made. At 2 ML Cu only a contrast minimum was observed at 2 ML Co and the magnetization distribution in the bottom layer was perfectly transferred to the top layer, presumbly via direct F coupling through gaps in the Cu spacer. The evolution of the angular $\boldsymbol{M}$ distribution with top Co layer thickness can be quantified somewhat by calculating pixel by pixel the orientation of $\boldsymbol{M}$ from the grey levels in the three component images and plotting it

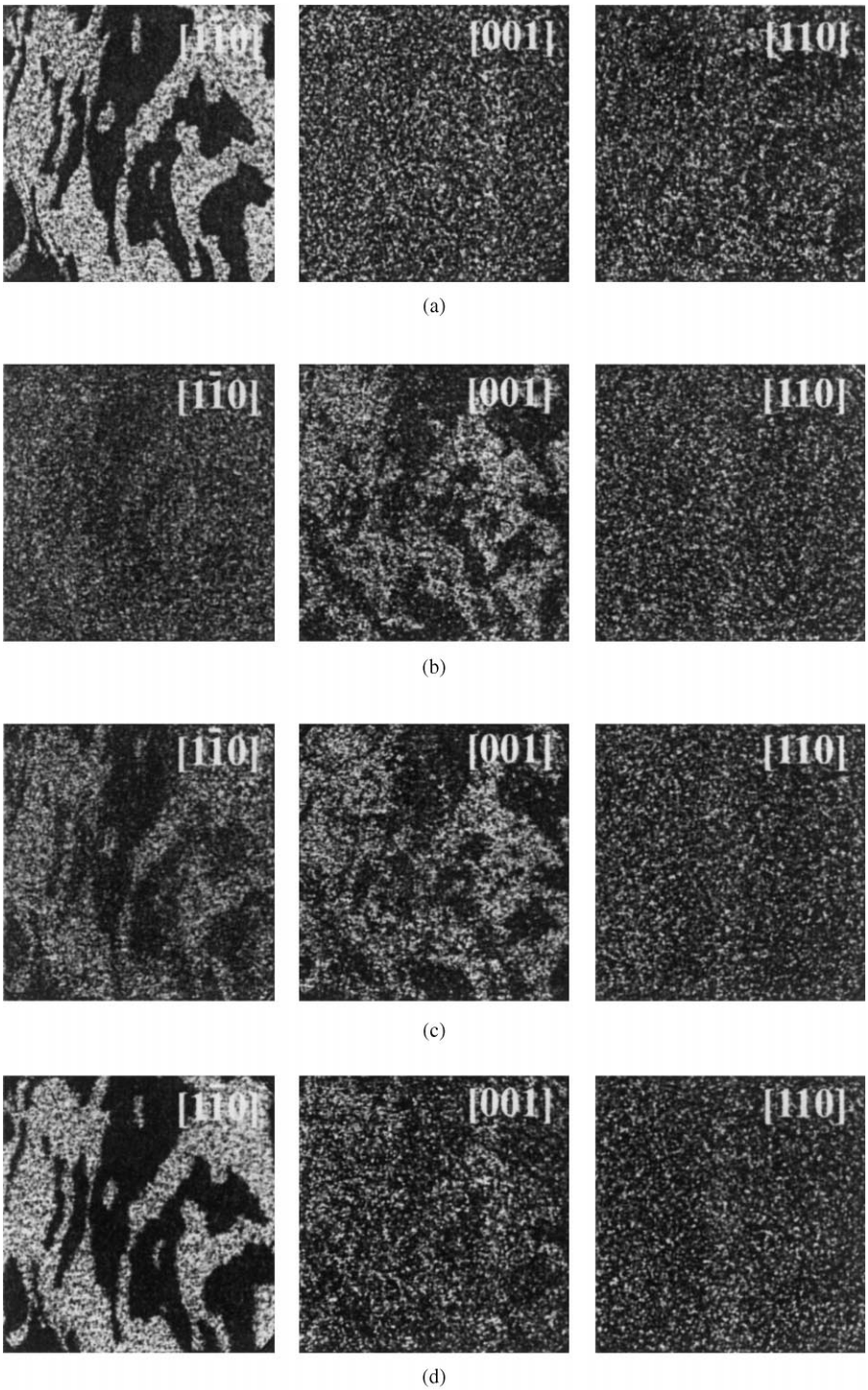

Fig. 1. Typical SPLEEM image series of a 7 Co/8 Cu/7 Co sandwich. (a) Uncovered bottom Co layer $\approx$ 8 Cu/7 Co. (b) 3 Co/8 Cu/7 Co. (c) 4 Co/8 Cu/7 Co. (d) 7 Co/8 Cu/7 Co. Electron energy $\approx$ 1.2 eV, field of view $\approx 6 \times 6\ \mu m^2$.

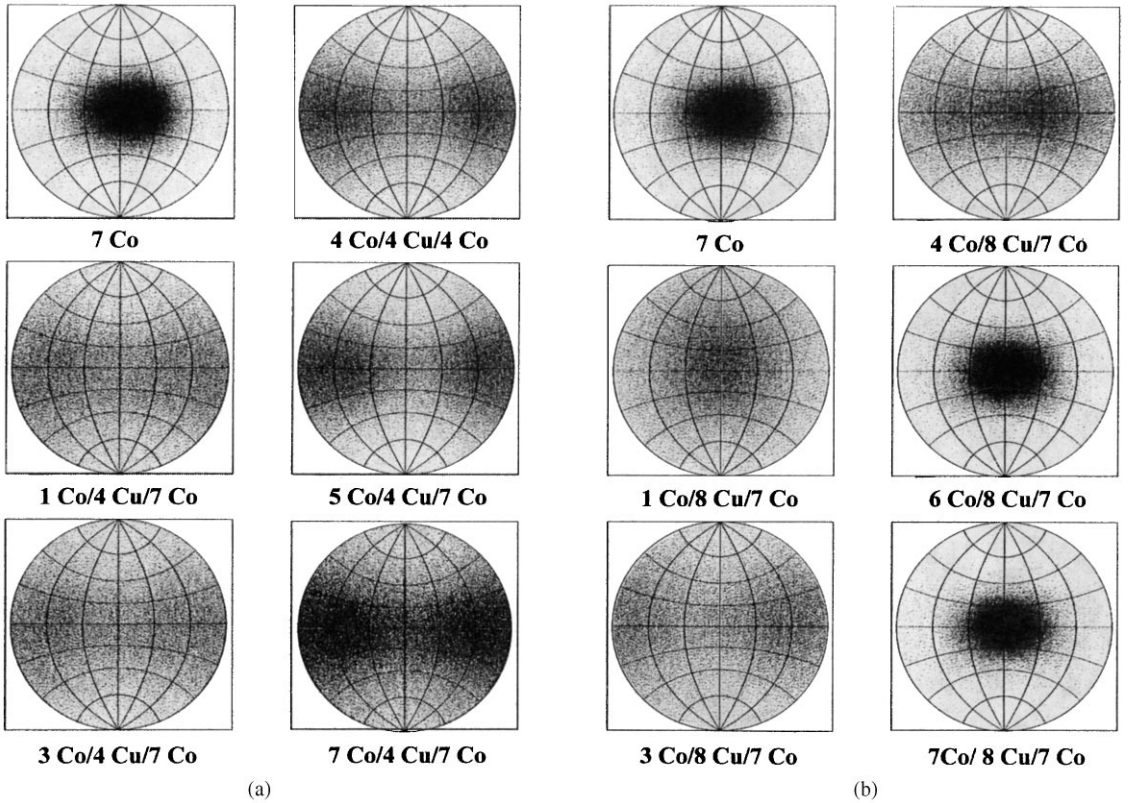

Fig. 2. Evolution of the angular $\boldsymbol{M}$ distribution with increasing thickness of the top Co layer (a) from a sandwich just below the AF coupling regime (4 ML Cu spacer), (b) from a sandwich close to the F coupling maximum (8 ML Cu spacer). Center of the projected unit sphere: [1 $\bar{1}$ 0], left side: [0 0 $\bar{1}$], right side: [0 0 1], top: [1 1 0], bottom: [$\bar{1}$ $\bar{1}$ 0].

in a locally orthogonalized projection of the unit sphere. This presentation of the angular $\boldsymbol{M}$ distribution is shown in Fig. 2. Series (a) has been taken at 4 ML Cu just below the AF coupling maximum, series (b) at 8 ML Cu within the F coupling regime. In both cases, the magnetization reappears preferentially in the W[0 0 1] direction but with increasing Co thickness two completely different $\boldsymbol{M}$ distributions develop: just below the AF coupling maximum the distribution has weak broad maxima near $\phi = 90^\circ$, in the F coupling region the angular $\boldsymbol{M}$ distribution develops a sharp maximum again at $\phi = 0^\circ$.

The dependence of the final spatial $\boldsymbol{M}$ distribution upon spacer thickness is illustrated by the series of images of Fig. 3 which shows in the left coulumn the in-plane $\boldsymbol{M}$ image of the bottom layer for reference, in the center the 0° image of the complete sandwich and on the right side the corresponding 90° image. At 3 ML Cu (a–c) there is only very weak fine-grained contrast in the center but pronounced contrast on the right indicating dominating biquadratic coupling. At 4 ML (d–f) the contrast in the center has increased somewhat but without recognizable F or AF coupling and the right image shows even stronger contrast than at 3 ML. Thus biquadratic coupling seems to be strongest between 3 and 4 ML. At 4.25 ML (g–i) and 4.5 ML (j–l) clear AF coupling is evident and the 90° image (right side) contrast is decreasing. This trend continues into the F coupling region as illustrated by the 7 ML spacer images (m–o). Calculation of the angular $\boldsymbol{M}$ distributions as described above gives a more quantitative picture of the

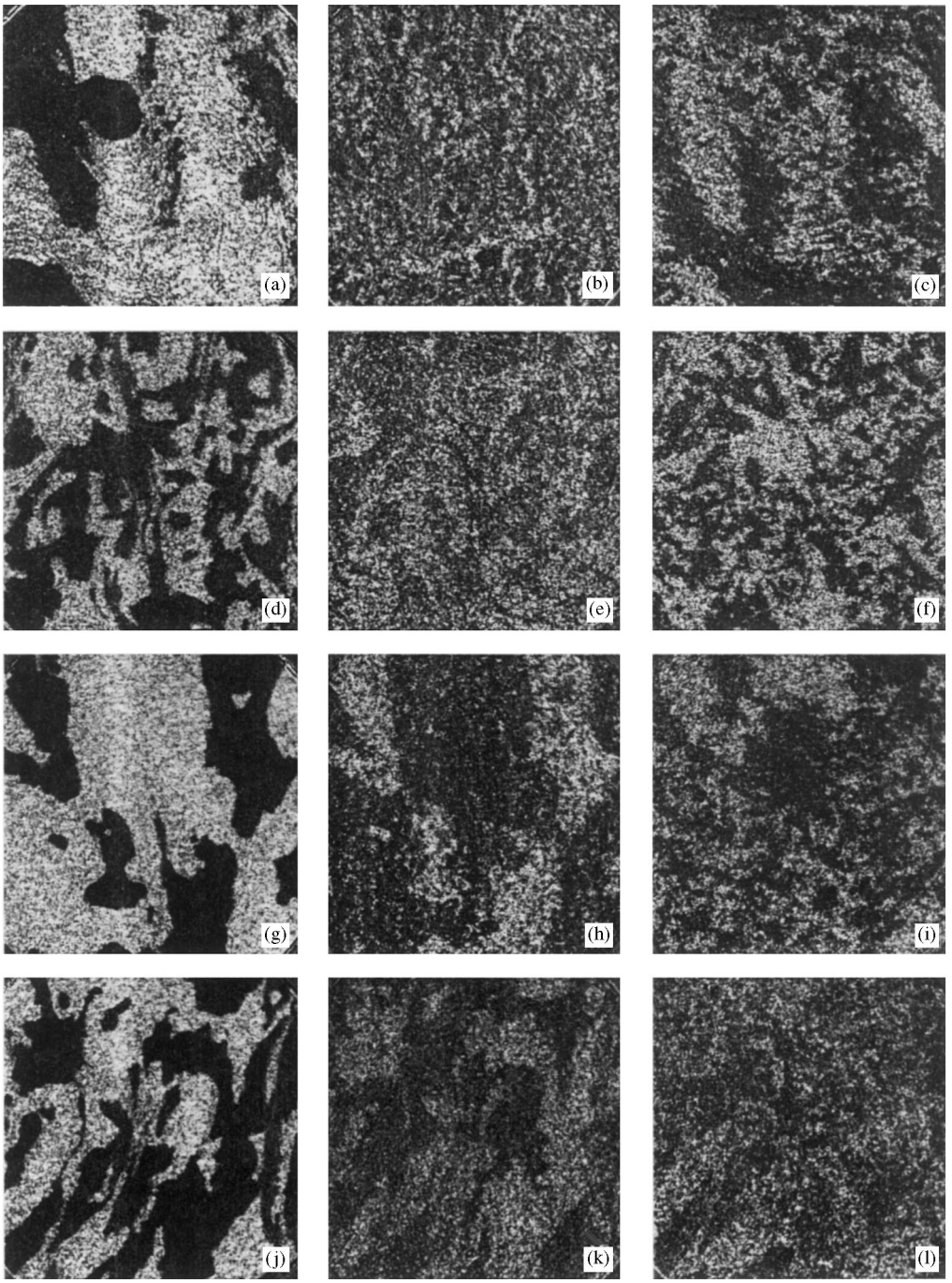

Fig. 3. Selected SPLEEM images illustrating the evolution of the domain structure of the completed sandwiches with Cu spacer thickness. The left column shows the in-plane images of the bottom Co layer which serve as a reference. The center column shows the images of the top Co layer taken with the same ***P*** direction (0° images), the right column the images with ***P*** in the perpendicular in-plane direction (90° images). The Cu spacer thickness is 3, 4, 4.25, 4.5, 7, 8 and 4.5 ML from top to bottom. The top Co layer is 6 ML thick in all cases. The last 4.5 ML Cu spacer sandwich was grown at 400 K. Electron energy ≈ 1.4 eV, field of view $\approx 6 \times 6\ \mu m^2$.

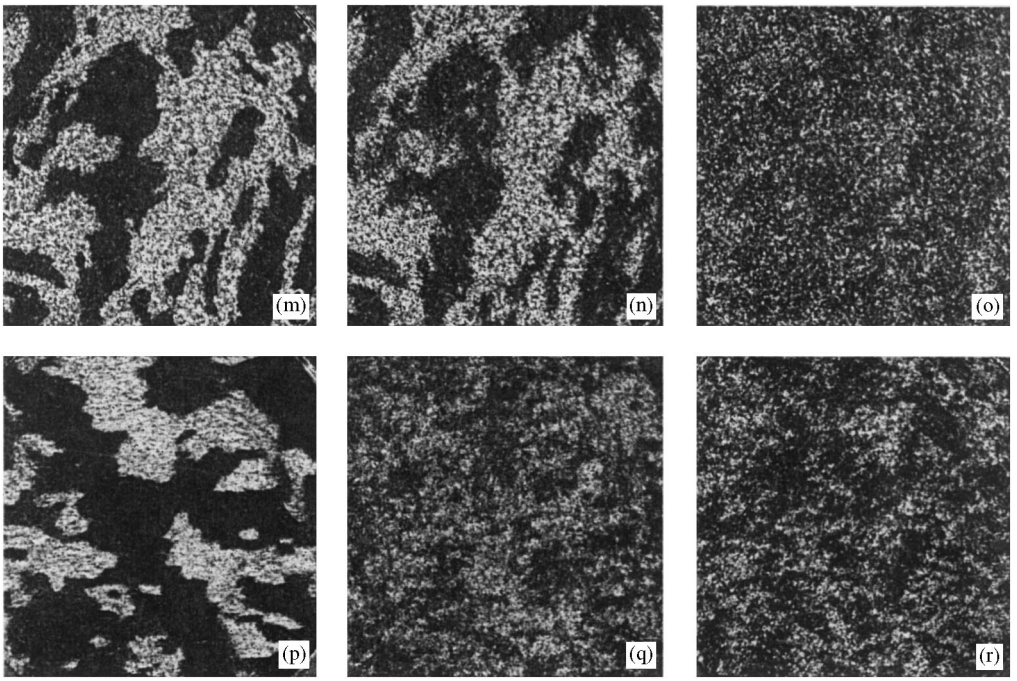

Fig. 3. Continued.

content of Fig. 3. Fig. 4 shows a section through the unit spheres of Fig. 2 along the equator for the complete sandwiches. This section gives the in-plane angular $\boldsymbol{M}$ distribution. Clearly, at 2, 6, 7 and 8 ML Cu the maxima occur at $\phi = 0^\circ$ and 180°, at 3 ML Cu at 90° and at 4 ML Cu at 100°. The difference between 3 and 4 ML is outside the limits of error and indicates a small bilinear component admixture at 4 ML to the nearly 100% biquadratic coupling at 3 ML. From Fig. 3g–Fig. 3l it is also clear that there is never pure AF coupling but always a mixture with biquadratic coupling.

In order to obtain some insight in how sensitive the coupling is to the deposition conditions the 4.5 ML spacer sandwich was also deposited at elevated temperature ($\approx$400 K) at which significantly larger Cu crystals grow than close to room temperture. Fig. 3q–Fig. 3r shows the $\boldsymbol{M}$ distribution of the complete sandwich. There is no relation with the domain structure of the bottom Co layer (Fig. 3p), thus no AF coupling, and both component images show very fine-grained structure. The difference

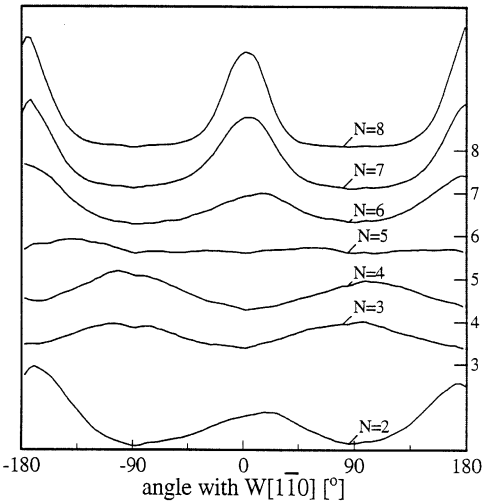

Fig. 4. In-plane angular $\boldsymbol{M}$ distributions in the completed (7 ML thick Co top layer) sandwiches. N is the spacer thickness in ML. The zeros of the curves have been shifted as indicated on the right hand side.

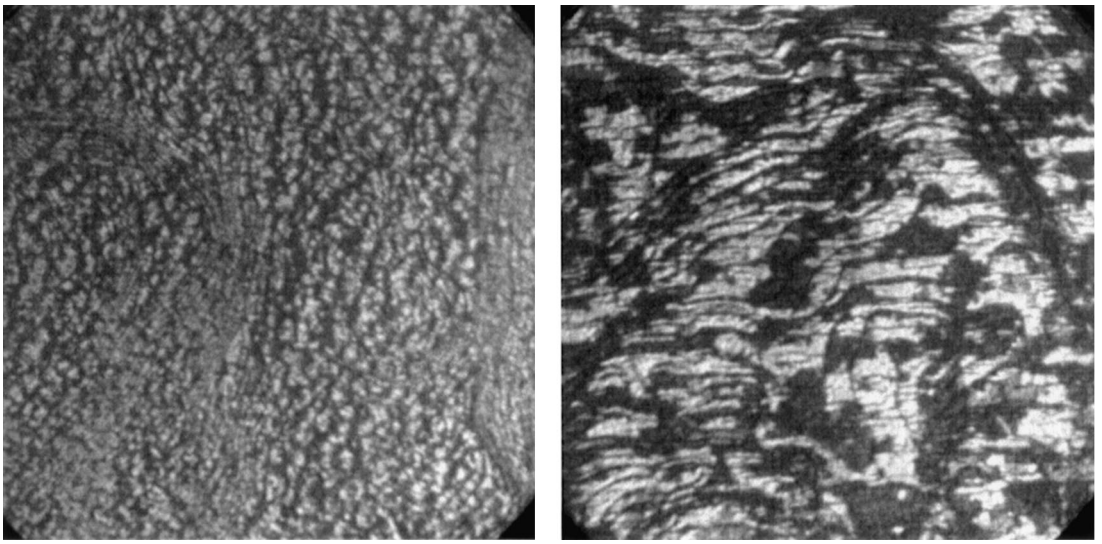

Fig. 5. Topographic images of 4.5 ML thick Cu spacer layers deposited close to room temperature (left side) and at elevated temperature (≈400 K, right side). The corresponding SPLEEM images are shown in Fig. 3j–Fig. 3l and in Fig. 3p–Fig. 3r.

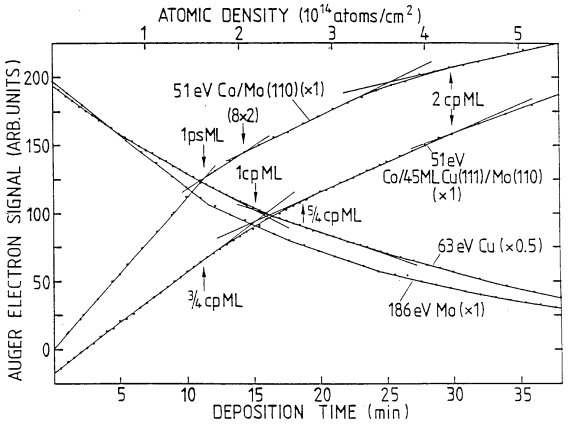

Fig. 6. Differentiated Auger electron signals of Co and of the substrate material (Mo, Cu) as a function of deposition time. Room temperature depositions with identical rates. ps and cp refer to pseudomorphic and close-packed monolayers on the Mo(1 1 0) surface. The continuous transition of the signals around 15 min show that the second monolayer starts to grow before the first monolayer is completed.

between the magnetic structures of the low and the high temperature deposits is clearly caused by the structural differences which are evident in the topographic images shown in Fig. 5.

4. Discussion

Before the discussion of the results some comments on the growth of Co on Cu(1 1 1) and of Cu on Co(0 0 0 1) have to be made. In the thermodynamic limit the growth mode of Co on Cu is not clear because the parameters which enter the growth mode criterion are not known accurately enough [14]. In the bulk, Co and Cu are immiscible but this does not exclude the formation of a surface or interface alloy. The experimental results are contradictory. Initial growth of bilayer islands in twin position has been reported on the basis of STM studies [15]. An even more three-dimensional growth has been deduced from low-energy ion scattering measurements from which it was concluded that only 40% of the Cu(1 1 1) surface were covered by Co at 1.2 ML thickness and only more than 80% at 3 ML Co [16]. On the other hand, there is strong evidence that there are no stacking faults in the first two monolayers in which the Co atoms are in FCC positions [17]. This shows that the growth mode depends sensitively upon the deposition conditions and on the state of the substrate surface used in the different experiments. In the present study the Co islands were too small and the

contrast too weak as to allow a clear distinction between monolayer versus bilayer growth and twinning versus nontwinning. However, the growth conditions were very similar to those used in earlier precise Auger electron spectroscopy (AES) studies which indicate initial monolayer growth followed by a slow transition to flat multilayer growth. Fig. 6 [18] shows the 51 eV Co AES signal on a Mo(1 1 0) surface and on a very flat Cu(1 1 1) layer on this substrate as a function of deposition time under identical conditions. Co grows on Mo(1 1 0) up to 2 ML layer-by-layer and continues to grow in a flat three level mode [19] which is also verified by LEEM on W(1 1 0) [20]. The AES curve for Co on Cu(1 1 1) is very similar with minor differences, which are due to differences in the back-scattering from the substrate. This is a clear indication of monolayer-by-monolayer growth, in agreement with many other studies [21].

The wetting of the Cu surface by one ML of Co is quite plausible: the atomic diameters of Co and Cu in the bulk are 2.506 and 2.556 Å, respectively. The surface layer wants to have a larger interatomic distance which is provided by the Cu substrate so that the misfit favors monolayer formation. In the reverse case, Cu on Co, the situation is different: the tendency to a larger interatomic spacing than in the bulk increases the surface stress and make layer-by-layer growth unfavorable. Indeed, LEEM/SPLEEM studies of Co layers with very thin Cu overlayers indicate that although a monolayer forms initially, the next layer grows via bilayer islands [22]. This is in apparent disagreement with a very recent study of the early stages of epitaxial growth of Cu on the (0 0 0 1) surface of bulk Co. In this study it was concluded that Cu grows approximately layer-like up to 4 ML and only thereafter forms three-dimensional islands [23]. However, it has to be kept in mind that in these experiments Cu was deposited without interruption and at much higher rate than here. Under these conditions growth is much more determined by kinetics than in the present work which was done closer to equilibrium, favoring the Stranski–Krastanov growth noticed also in Ref. [23]. The subsequent discussion is, therefore, based on the model of a relatively flat bottom three-level Co/Cu interface with large terraces and a somewhat rougher top Cu/Co interface with small terraces.

The second point which needs to be addressed before the discussion of the images concerns the interaction of the spin-polarized electrons with the target. The information depth of LEEM/SPLEEM depends upon the mean free path (MFP) of the electrons and the image contrast is strongly influenced by quantum size effects (QSE). Both, MFP and QSE are spin-dependent. Very little is known about the MPF at the low energies used in SPLEEM (1–2 eV). Energy-averaged values for slow secondary electrons show a linear dependence upon the number of holes in the d band. The value for Co is about 8 Å [24]. For Cu a MFP of 10 Å has been reported originally [25] which is abnormally small for a metal with a filled d shell. A more recent value is 19 Å [24]. Whatever the exact values of the MFPs may be, SPLEEM image analysis must take into account the possibility that the sampling depth may be as much as several 10 Å. The spin dependence of the MFP brings an additional complication. The MFPs for spin-up and spin-down electrons differ increasingly with decreasing energy if ineleastic scattering dominates the MFP [26]. At very low energies the MFP for spin-up electrons may be several times larger than that for spin-down electrons [26]. For electrons 1.5 eV above the Fermi level a MFP of 14.7 Å for spin-up electrons and of 5.4 Å for spin-down electrons has been deduced from spin-polarized photoemission measurements of Co on Cu, assuming a MFP of 14 Å in Cu [27].

The SPLEEM images shown in Section 3 are taken between 1 and 2 eV above the vacuum level, that is in an energy range in which spin-up electrons can couple to allowed states in the volume but not spin-down electrons which, therefore, can exist in the crystal only as evanescent waves. However, these have a relatively large decay length (small imaginary part of k) because the band gap in the [0 0 0 1] direction is wide and the energy of the electrons is close to the band edge [9]. As a consequence, the spin-down electrons travel far enough to loose energy – to be 'absorbed' – which reduces their reflected intensity I_- and, thus, the magnetic contrast. For the MFP in Co mentioned above (5.4 Å) I_- is reduced to 47, 22 and 5% of the intensity in the absorption free case in a 1, 2 and 4 ML thick film due to inelastic scattering on the

way in and out. In Cu, on the other hand, absorption is much weaker so that Cu overlayers weaken the magnetic contrast much less than Co overlayers, in qualitative agreement with the SPLEEM observations.

Finally, the QSE which has long been used in LEEM for the determination of film thickness differences, has a major influence on the image contrast in SPLEEM. This is due to the fact that the k values, that is the wavelengths for a given energy, differ for spin-up and spin-down electrons due to the exchange splitting of the band structure $E(\boldsymbol{k})$. As a consequence the interference conditions in the quantum well differ and the asymmetry shows strong oscillations as a function of energy and film thickness. This has been well demonstrated experimentally for Co layers on W(1 1 0) [9,12,28] and theoretically by spin-polarized LEED calculations [29].

Considering all these aspects, it is obvious that SPLEEM images have to be analyzed with considerable caution as long as no theory is available which takes proper account of these aspects or as long there is not enough empirical experience in the analysis. While the local direction of $\boldsymbol{M}$ can be determined unambiguously – except possibly for the sign due to QSE contrast reversals at certain energies with increasing thickness [30] – the magnitude of $\boldsymbol{M}$ cannot be determined at present. In spite of these limitations valuable information can be extracted from the images shown in Figs. 1–5. The image interpretation will be based on the assumption – based on the strong absorption of spin-down electrons in Co discussed above – that all images with more than 3 ML Co in the top layer show only the magnetization of the top layer.

For comparison with the present data, some results from the literature should be recalled. The average value – obtained from many studies of the Co/Cu/Co system – of the Cu thickness at which the first maximum of the magnetoresistance or of the saturation field occurs is 4.15 ML, that of the second maximum 9.2 ML. These maxima are attributed to AF coupling, that is to negative extrema of the bilinear coupling parameter J_1. AF coupling is believed to occur only in part of the layer system, the majority being F coupled. The maximum of the F coupling which can be deduced from these macroscopic measurements occurs at about 7.6 ML Cu. A zero of J_1 at 2.5–3 ML is suggested by some experiments. The theoretical value for the J_1 oscillation period is 4.50 ML [31] which would give a zero of J_1 at about 3.4 ML.

The fact mentioned earlier that at 2.5 ML the Cu layer consists of double layer islands on top of the first Cu layer explains why the F contrast is not reduced as much at 2 ML Co by inelastic scattering as in the case of thicker Cu spacers before the contrast increases again with increasing Co thickness: there is some ferromagnetic coupling through the first monolayer in the gaps between the double layer islands. The weak contrast which becomes visible in the 90° image above 5 ML Co shows, however, that there is already a biquadratic contribution to the coupling. At 3 ML Cu biquadratic coupling is dominating as seen in Fig. 3a–Fig. 3c. The domains in the parallel (0°) image are so small that they are hardly recognizable in the noise after it become visible at 3 ML Co and are uncorrelated to the domain structure of the bottom Co layer which suggests that the bilinear coupling parameter $J_1 \approx 0$. The large domains in the 90° image interestingly show a certain correlation which is determined by the substrate step structure. At 4 ML Cu there is still no clear correlation with the domain structure in the substrate in the 0° image but the image is less fine-grained (Fig. 3e). The contrast in the 90° image (Fig. 3f) is still larger than that in the 0° image but the domain size is now smaller than at 3 ML. This indicates that biquadratic coupling is still dominating but weaker than at 3 ML Cu.

The equal contrast in the two images at 4.25 ML Cu (Fig. 3h and Fig. 3i) and the somewhat weaker contrast in the 90° image than in the 0° image at 4.5 ML Cu (Fig. 3k and Fig. 3l) show the decreasing influence of the biquadratic coupling near the AF maximum believed to be between these two thicknesses. The AF coupling is evident from the comparison of Fig. 3g and Fig. 3h and of Fig. 3l and Fig. 3m. At 5 ML Cu (not shown) there is already weak F coupling in the 0° image with good correlation to the bottom layer domain structure but weak contrast which is comparable again with the 90° contrast. Thus J_1 is positive but small. At 6 ML Cu

(not shown) there is already strong F coupling again which persits up the the largest spacer thickness studied (9 ML) as illustrated in Fig. 3n and Fig. 3o for 7 ML Cu. Interesting are the changes in the 90° images: at 6 ML Cu the contrast is still increasing with Co layer thickness in the same manner as in the 0° images but at 7 ML CU and in particular at 8 ML Cu it passes through a maximum at 3–4 ML Co while the 0° contrast is still weak and increasing. This trend is still noticeable though weaker at 9 ML Cu. At 7 and 8 ML Cu the 90° contrast is nearly vanishing which is compatible with a maximum of J_1 close to these thicknesses.

This dependence of J_1 is in good agreement with that derived in the past from the macroscopic measurements but there is a major difference in the sign of the coupling: The macroscopic measurements which all involve an external field indicate always some AF coupling above 3 ML Cu while the microscopic zero field data presented here show only F coupling from 6 ML Cu onwards in the 0° images. Apparently, the GMR is not due to AF coupling but caused by the breakup of the domains in subdomains with wrinkled magnetization due to the presence of biquadratic coupling. This suggestion is supported by the observation that the biquadratic contribution is smallest at the minimum of the magnetoresistance between 7 and 8 ML Cu and is in partial agreement with the conclusion that the GMR is due to 90° coupling [32,35]. Interesting and not understood is the fact that the top layer develops at 6 ML Cu and above initially, that is at 3 ML Co, predominantly 90° magnetization while the F coupling is still building up, and then is increasingly replaced by F coupling with increasing thickness. Apparently the ratio of interface roughness to average Co layer thickness plays an important role for the magnitude of the biquadratic coupling.

Finally, the results obtained during the growth of the sandwich with 4.5 ML Cu at the elevated temperture have to be discussed yet. Fig. 3p–Fig. 3r shows that the final domain structure has no relationship to that of the bottom layer and that 0° and 90° image have the same contrast without preferred contrast levels, indicating that there is no preferred magnetization direction. The cause for this loss of magnetic order is evident from the evolution of the images during the growth. Just as in the case of the 2.5 ML Cu sandwich grown at room temperature, the original domain structure is still well visible at 2 ML Co where it is barely noticeable in the other sandwiches. At 3 ML Co there is practically no contrast in the 0° image while in the 90° image the first signs of the contrast seen in Fig. 3r already develop. This can be understood in the same manner as the 2.5 ML images: the Cu layer is broken up into large crystals which allows close proximity of the top layer to the bottom layer in between them, attenuating initially the domain structure of the bottom layer only partially. As soon as the top layer becomes magnetic (at 3 ML Co) it develops a fine grained magnetization which is determined by the roughnees of the interface, with locally strongly varying coupling. The magnetoresistance in this case is now mainly due to the fine grains with varying magnetization directions.

5. Summary

The microscopic view of the effects of interlayer coupling in zero field presented here shows how complex the resulting domain structure is. The domain structure of the bottom layer is certainly strongly influenced by the topography of the substrate as shown elsewhere [11] but the domains are large enough so that the local coupling may be considered to be representative also for the more ideal case of very large domains. The results confirm in general the conclusions drawn from macroscopic measurements in an external field regarding the coupling but differ also in several aspects. In particular, the strong dependence of the type of coupling – bilinear or biquadratic – upon the thickness of the spacer layer and of the top magnetic layer is new. It appears that biquadratic coupling builds up faster with increasing top magnetic layer thickness than bilinear coupling, except for spacer thicknesses close to maximum F coupling, and disappears with increasing bilinear coupling. Below the thickness with maximum AF coupling biquadratic coupling dominates even at larger top layer thicknesses. That these effects have not been noticed before may be due to differences in the film

structure but at least also in part due to the fact that the zero magnetization configuration in measurements in an external field ($H = H_c$) is quite different from that of the virgin state ($H = 0$). Another possible reason is that biquadratic coupling produces clear domain patterns in SPLEEM while Lorentz microscopy shows only wavy boundaries with relatively low contrast [33]. An additional advantage of SPLEEM is that it can be done on bulk substrates and during film growth.

Acknowledgements

The authors acknowledge the loan of the SPLEEM equipment by the TU Clausthal, Germany.

References

[1] P. Bruno, Phys. Rev. B 52 (1995) 411.
[2] B.A. Jones, IBM J. Res. Dev. 42 (1998) 25.
[3] B. Heinrich, J.F. Cochran, Adv. Phys. 42 (1993) 523.
[4] B. Heinrich, J.C.A. Bland (Eds.), Ultrathin Magnetic Structures II, Springer, Berlin, 1994, Ch. 2.
[5] R.F.C. Farrow, IBM J. Res. Dev. 42 (1998) 43.
[6] J. Camarero et al., Phys. Rev. Lett. 76 (1996) 4428.
[7] W. Kuch, et al., J. Magn. Magn. Mater. 170 (1997) L13.
[8] J. Camarero et al., Phys. Rev. Lett. 73 (1994) 2448.
[9] E. Bauer, in: S. Amelinckx, et al., (Eds.), Handbook of Microscopy, VCH, Weinheim, 1997, p. 751.
[10] E. Bauer, Rep. Prog. Phys. 57 (1994) 895.
[11] T. Duden, E. Bauer, Phys. Rev. Lett. 77 (1996) 2308.
[12] E. Bauer et al., J. Magn. Magn. Mater. 156 (1996) 1.
[13] T. Duden, E. Bauer, Rev. Sci. Instrum. 66 (1995) 2861.
[14] J.H. van der Merwe, E. Bauer, Phys. Rev. B 39 (1989) 3632.
[15] J. de la Figuera et al., Phys. Rev. B 47 (1993) 13043.
[16] A. Rabe et al., Phys. Rev. Lett. 73 (1994) 2728.
[17] M. Hochstrasser et al., Phys. Rev. B 50 (1994) 17705.
[18] M. Tikhov, E. Bauer, Unpublished.
[19] M. Tikhov, E. Bauer, Surf. Sci. 232 (1990) 73.
[20] T. Duden et al., Unpublished
[21] Ch. Rath et al., Phys. Rev. B 55 (1997) 10791.
[22] T. Duden, E. Bauer, Phys. Rev. B, in press.
[23] J.E. Prieto et al., Surf. Sci. 401 (1998) 248.
[24] H.C. Siegmann, Surf. Sci. 307–309 (1994) 1076.
[25] D.T. Pierce, H.C. Siegmann, Phys. Rev. B 9 (1974) 4035.
[26] F. Passek, M. Donath, K. Ertl, J. Magn. Magn. Mater. 159 (1996) 103.
[27] J.C. Groebli, D. Oberli, F. Meier, Phys. Rev. B 52 (1995) R13095.
[28] K. Wurm, M.S. Thesis, TU Clausthal, 1994.
[29] T. Scheunemann et al., Solid State Commun. 30 (1997) 1.
[30] H. Poppa et al., MRS Symp. Proc. 313 (1993) 219.
[31] P. Bruno, C. Chappert, Phys. Rev. Lett. 67 (1991) 1602.
[32] Z.J. Yang, M.R. Scheinfein, Appl. Phys. Lett. 66 (1995) 236.
[33] J.D. Kim et al., J. Appl. Phys. 76 (1994) 6513.
[34] E. Bauer, in: S. Amelinckx, et al., (Eds.), Handbook of Microscopy, VCH, Weinheim, 1997, p. 487.
[35] Z.J. Yang, M.R. Scheinfein, Phys. Rev. B 52 (1995) 4263.
[36] E. Bauer, W. Telieps, in: A. Howie, U. Valdré (Eds.), Surface and Interface characterization by Electron Optical Methods, Plenum, New York, 1988, p. 195.